Dissipation and entropy production in deterministic heat conduction of quasi-one-dimensional systems

Gary P. Morriss and Daniel P. Truant*
School of Physics, University of New South Wales, Sydney, New South Wales 2052, Australia
(Received 23 April 2013; published 28 June 2013)

We explore the consequences of a deterministic microscopic thermostat-reservoir contact mechanism. With different temperature reservoirs at each end of a two-dimensional system, a heat current is produced and the system has an anomalous thermal conductivity. The microscopic form for the local heat flux vector is derived and both the kinetic and potential contributions are calculated. The total heat flux vector is shown to satisfy the continuity equation. The properties of this nonequilibrium steady state are studied as functions of system size and temperature gradient, identifying key scaling relations for the local fluid properties and separating bulk and boundary effects. The local entropy density calculated from the local equilibrium distribution is shown to be a very good approximation to the entropy density calculated directly from the velocity distribution even for systems that are far from equilibrium. The dissipation and kinetic entropy production and flux are compared quantitatively and the differing mechanisms discussed within the Bhatnagar-Gross-Krook approximation. For equal-temperature reservoirs the entropy production near the reservoir walls is shown to be proportional to the local phase space contraction calculated from the tangent space dynamics. However, for unequal temperatures, the connection between local entropy production and local phase space contraction is more complicated.

DOI: 10.1103/PhysRevE.87.062144 PACS number(s): 05.20.Jj, 05.45.Jn, 05.70.Ln

I. INTRODUCTION

The study of heat conduction in low-dimensional systems has concentrated on one-dimensional lattices [1–4] and simplified Hamiltonian models that are amenable to solution [5–7]. The Hamiltonian models often consist of energy storage devices which couple to each other through the motion of tracer particles that carry the energy. Exceptions to this have been rare, but one of these is the study of particle-based systems using hard disks by Deutsch and Narayan [8], and others [9]. The other common features of these model systems are that the thermal reservoirs are stochastic and are thus sources of particles with velocities chosen from some distribution and the reservoir is not mechanically coupled to the system. This element of randomness has limited the approaches that could be used to study heat conduction as a dynamical system [10].

In 2007 a new deterministic thermal reservoir was introduced that coupled the quasi-one-dimensional system of hard disks to temperature reservoirs by changing the collision rule at the reservoir boundary [11]. For a collision with a reservoir boundary the tangential y component of momentum is unchanged but the normal x component after collision becomes

$$p_x' = \epsilon p_{res} - (1-\epsilon)p_x, \tag{1}$$

where p_{res} is a reservoir momentum related to the reservoir temperature by $p_{res} = \sqrt{2T_{res}}$ and ϵ is a reservoir coupling parameter. As $\epsilon \to 0$ the system decouples from the reservoir and the boundary becomes a hard wall, and as $\epsilon \to 1$ the incoming momentum is replaced by the reservoir momentum. A recent study of this system in contact with two reservoirs of the same temperature [12] has shown that the active mechanical coupling leads to entropy production near each reservoir which then flows into the reservoir. These effects are local and involve a limited number of boundary layer particles regardless of the system size.

Molecular dynamics simulations have proved a very effective means of testing theoretical approaches to the study of fluids both in equilibrium, and in nonequilibrium steady states [13]. Given a particular atomic pair interaction, the results are free of approximations, with an accuracy limited only by statistical considerations. It is usual to use the equipartition theorem to define the *kinetic temperature*, so in a system of N particles in d spatial dimensions the translational kinetic energy is $\frac{kT}{2}$ per degree of freedom. We define instantaneous local temperatures for each particle so that in two spatial dimensions $T_{i,x} = p_{i,x}^2/m$ and $T_{i,y} = p_{i,y}^2/m$, and then the instantaneous system temperature is

$$T = \frac{1}{2N}\sum_{i=1}^{N}(T_{i,x} + T_{i,y}) = \frac{1}{N}\sum_{i=1}^{N}\frac{\mathbf{p}_i^2}{2m}. \tag{2}$$

In the absence of a temperature gradient the average $\langle T\rangle$ gives the system temperature, but when there is a temperature gradient the local time averages $\langle T_{i,x}\rangle$ and $\langle T_{i,y}\rangle$ give the local temperatures which will be used to determine the temperature profile inside the system. The difference between the local components of the local temperature can be used to give a measure of the deviation from local thermodynamic equilibrium. We use $T_{i,x}$ and $T_{i,y}$ to define a local *operational* temperature for a nonequilibrium system, but it is more usual to attempt to connect the average *local* kinetic temperature and the *local* thermodynamic temperature. The relationship between this *kinetic* and the *thermodynamic* temperature is only beginning to be explored [14–17].

For a quasi-one-dimensional (QOD) system we can extend the idea of a kinetic temperature for a single atom to define the *local kinetic temperature* in the average volume element occupied by the particle, as the order of the particles is fixed. Then we extend this idea to define other local thermodynamic properties using the properties of the particle that occupies the

*dan.truant@gmail.com

volume element. In particular the velocity distribution of the particle can be used to define the velocity distribution of the volume element and then the thermodynamic properties that are derived from it.

For equilibrium systems we expect a well-defined thermodynamic limit so that average properties converge with increase of the system size. However, for nonequilibrium systems a thermodynamic limit is not useful. If the temperatures of the two reservoirs are fixed and the system size is increased then the temperature gradient goes to zero. If the gradient is fixed then it is usual to observe a hydrodynamic instability at some threshold system size where the system behavior abruptly changes. Given this difficultly we consider sequences of *equivalent* nonequilibrium systems of different sizes or different gradients to obtain scaling relations which remain correct in the regime before the onset of hydrodynamic instability.

II. THE MODEL SYSTEM

In this section we introduce a simple deterministic microscopic model for thermal coupling of a system of hard disks to a reservoir which can be used with either an equilibrium system or a nonequilibrium steady state, to supply or remove heat. As this microscopic model couples mechanically and deterministically to the system it may be probed as would be a standard dynamical system, and energy and kinetic entropy flows calculated numerically without approximations. The mechanism has been introduced previously [11], and studied by computer simulation and kinetic theory [18,19].

A. System dynamics

The quasi-one-dimensional system introduced in [20] can be modified to interact with an idealized *heat reservoir* in a deterministic and reversible way, to study both heat conduction in low-dimensional systems [3] and the Lyapunov spectra and mode structure. The deterministic reservoir allows the calculation of the usual dynamical system properties as well as the thermodynamic properties. This system contains hard disks of diameter σ (which we set equal to 1) in a narrow channel that does not allow the disks to change their positional order; see Fig. 1. Therefore any property of particle i can be associated with the same local property in the volume element $V_i = L_y(\langle x_{i+1} - x_{i-1}\rangle)/2$, centered at the average position of particle i, $\langle x_i \rangle$; thus, for example, the local density is the inverse of the average volume occupied by the particle, $\rho_i = 1/V_i$.

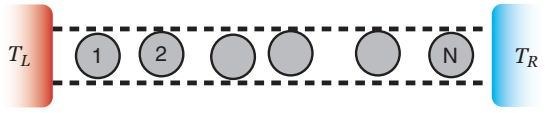

FIG. 1. (Color online) Schematic presentation of an N-hard-disk quasi-one-dimensional system. The height L_y is sufficiently small that the disks cannot pass one another. We choose the coordinate origin to be located at the bottom left corner of the system, and the periodic upper and lower system boundaries at $y = 0, L_y$ are denoted by dashed lines. The boundaries at $x = 0$ and $x = L_x$ are the hard walls of the reservoirs so this is an (H,P) QOD system.

The equations of motion connecting the QOD system to the two reservoirs, one on the left-hand (LH) side at $x = 0$ and the other on the right-hand (RH) side at $x = L_x$ define the *thermal contact* so when a particle collides with a reservoir wall the normal component of the momentum of the particle p_x is changed as given in Eq. (1). For the LH reservoir $p_{res} = p_L$ is the fixed value of the reservoir momentum and for the RH reservoir $p_{res} = -p_R$ (note that the reservoir momentum is always directed into the system). The reservoir coupling parameter ϵ represents the strength of the coupling of the reservoir to the system. If $\epsilon = 0$ there is no interaction with the reservoir, and if $\epsilon = 1$ the incoming momentum is completely replaced by the reservoir momentum. Here we use an intermediate value of $\epsilon = 0.5$ which provides an effective mix of the incoming momentum with the reservoir momentum. The system has a volume $V = L_x L_y$ with a fixed width of $L_y = 1.15\sigma$, and then L_x varies with the number of particles N to give the desired density $\rho = N\sigma^2/(L_x L_y)$. As the QOD system is narrow enough to prevent particles interchanging their positions, $L_y < 2\sigma$, the order of the particles remains fixed (both σ and the mass m are set to 1). The temperature profile is determined from the average components of the kinetic temperature of each particle [the average of Eq. (2)].

To produce a nonequilibrium steady state it is sufficient to have reservoirs of different temperatures on each side of the QOD system. The energy entering the system from a boundary with reservoir momentum p_{res} during a collision with a particle of incoming momentum p_x is given by

$$\Delta e_I = \frac{1}{2}\left(p_x'^2 - p_x^2\right) = \frac{\epsilon}{2}\left[\epsilon p_{res}^2 + 2(\epsilon - 1)p_{res}p_x + (\epsilon - 2)p_x^2\right]. \quad (3)$$

The time average of this quantity gives the flux of energy *into* the system so for a total system energy balance Δe_L must be equal in magnitude but opposite in sign to Δe_R. The energy flux is controlled by both p_{res} and the value of ϵ, going to zero as $\epsilon \to 0$ and the reservoirs become disconnected from the system.

We choose the temperatures of the two reservoirs independently, so the temperature of the left-hand-side reservoir is $T_L > 2$ and varies, and the temperature of the right-hand-side reservoir is kept constant at $T_R = 2$. This produces a temperature gradient of $\nabla T = (T_R - T_L)/L_x$ so heat will flow from the left-hand reservoir to the right-hand reservoir. An overview of simulation state points is given in Table I.

B. Tangent space dynamics

The tangent space dynamics changes due to the changed collision rule at each boundary [21] so that for a particular

TABLE I. The simulation state points. For each density ρ a small and a large temperature gradient are considered. Generally, $T_R = 2$ and groups of simulations are carried out with either ∇T fixed and varying N (or equivalently ρ) or N fixed and varying ∇T.

ρ	Small ∇T	Large ∇T
0.03	−0.000431	−0.01380
0.8	−0.01150	−0.3680

reservoir we have

$$\delta x' = \left(\epsilon \frac{p_{res}}{p_x} + (\epsilon - 1)\right)\delta x, \tag{4}$$

$$\delta p_x' = (\epsilon - 1)\delta p_x, \tag{5}$$

where p_{res} is the value of the reservoir momentum. Notice that both p_L/p_{x1} and p_R/p_{xN} are negative so the sign of $\delta x'$ is opposite that of δx.

The time evolution of the QOD system in tangent space is an infinite product of pairs of tangent matrices for a free flight F_i and a collision C_i. The tangent space dynamics for an arbitrary tangent vector $\delta\Gamma(0)$ can be written as $\delta\Gamma(t) = M(t)\delta\Gamma(0)$ where $M(t)$ is a product of F and C matrices and the Lyapunov exponents are the logarithms of the eigenvalues of

$$\Lambda = \lim_{t\to\infty}[M(t)^T M(t)]^{1/2t}. \tag{6}$$

For any free flight or particle-particle collision the tangent matrix has a determinant that is equal to one. Only wall-particle collision matrices have a determinant that depends upon ϵ and differs from 1 so the dynamics becomes dissipative. The dissipation from a single collision with a reservoir d_I is given by the determinant of the wall collision matrix C_I^W as

$$d_I = \det C_I^W = (\epsilon - 1)\left((\epsilon - 1) + \epsilon \frac{p_{res}}{p_x}\right), \tag{7}$$

where p_x is the incoming momentum of the colliding particle. Note that the determinant approaches 1 as $\epsilon \to 0$, or as the wall becomes purely reflective, and as p_{res}/p_x is negative, both terms in Eq. (7) are negative ($0 \leqslant \epsilon < 1$), so their product $d_I > 0$. Combining Eqs. (6) and (7), the sum of the Lyapunov exponents for the system becomes

$$\sum_{j=1}^{2dN} \lambda_j = \ln[\det(\Lambda)] = \nu_L\langle d_L\rangle + \nu_R\langle d_R\rangle, \tag{8}$$

where ν_I is the collision frequency for reservoir I. As $\det C_I^W$ depends on p_x for both reservoirs, the angular brackets represent an average over the incoming distribution of p_x which in itself depends on the values of p_{res}. Further, we can calculate separately the components of dissipation associated with each reservoir, and this gives more local information than is available from the sum of Lyapunov exponents.

C. Microscopic heat flux vector

For a system of spherical particles the microscopic representation for the instantaneous local heat flux vector at position $\mathbf{r}$ and at time t is given by [13,22]

$$\mathbf{J}_Q(\mathbf{r},t) = \sum_{i=1}^{N} U_i \mathbf{v}_i \delta(\mathbf{r} - \mathbf{r}_i) - \frac{1}{2}\sum_{i,j}^{N} \mathbf{r}_{ij}\mathbf{F}_{ij}\cdot[\mathbf{v}_i + \mathbf{u}(\mathbf{r}_i) - \mathbf{u}(\mathbf{r})] \times \int_0^1 d\lambda\,\delta(\mathbf{r} - \mathbf{r}_i - \lambda\mathbf{r}_{ij}), \tag{9}$$

where $U_i = \frac{1}{2}m[\mathbf{v}_i - \mathbf{u}(\mathbf{r})]^2$ is the internal energy of particle i, $\mathbf{u}(\mathbf{r})$ is the local streaming velocity at $\mathbf{r}$, and $\mathbf{u}(\mathbf{r}_i)$ is the local streaming velocity at the position of particle i. For this system the local streaming velocity is zero everywhere. We define the vectors $\mathbf{r}_{ij} = \mathbf{r}_j - \mathbf{r}_i$ and $\mathbf{p}_{ij} = \mathbf{p}_j - \mathbf{p}_i$. For hard core particles the interaction force is an impulse $\mathbf{F}_{ij} = (\hat{\mathbf{r}}_{ij}\cdot\mathbf{v}_{ij})\hat{\mathbf{r}}_{ij}\delta(t - t_{ij})$, where t_{ij} is the time at which a collision occurs between particles i and j, and $\hat{\mathbf{r}}_{ij}$ is the unit vector in the direction of $\mathbf{r}_{ij}$; therefore Eq. (9) becomes

$$\mathbf{J}_Q(\mathbf{r},t) = \sum_{i=1}^{N} U_i \mathbf{v}_i \delta(\mathbf{r} - \mathbf{r}_i) - \frac{1}{2}\sum_{i,j}^{N} \hat{\mathbf{r}}_{ij}(\hat{\mathbf{r}}_{ij}\cdot\mathbf{v}_{ij})\hat{\mathbf{r}}_{ij}\cdot(\mathbf{v}_i + \mathbf{v}_j)\delta(t - t_{ij}) \times \int_0^1 d\lambda\,\delta(\mathbf{r} - \mathbf{r}_i - \lambda\mathbf{r}_{ij}). \tag{10}$$

Notice that if $\mathbf{v}_i + \mathbf{v}_j = \mathbf{0}$ there is no collisional energy transfer so the transfer of energy is correlated with the fluctuations of the pair momentum away from zero. In the integral, the δ function moves along a line from the position of particle i, $\mathbf{r}_i$, to the position of particle j, $\mathbf{r}_j$, as λ goes from 0 to 1, so a reasonable proposition is to assign half the potential contribution to each particle. This is analogous with assigning half the potential energy of interaction to each particle. We can make this more solid by considering the one-strip approximation to the integral, that is, $\frac{1}{2}\Delta[\delta(\mathbf{r} - \mathbf{r}_i) + \delta(\mathbf{r} - \mathbf{r}_j)]$ where the strip width is $\Delta = ||\hat{\mathbf{r}}_{ij}|| = 1$. Then Eq. (10) becomes

$$\mathbf{J}_Q(\mathbf{r},t) = \sum_{i=1}^{N} U_i \mathbf{v}_i \delta(\mathbf{r} - \mathbf{r}_i) - \frac{1}{4}\sum_{i,j}^{N} \hat{\mathbf{r}}_{ij}(\hat{\mathbf{r}}_{ij}\cdot\mathbf{v}_{ij})\hat{\mathbf{r}}_{ij}\cdot(\mathbf{v}_i + \mathbf{v}_j)\delta(t - t_{ij}) \times [\delta(\mathbf{r} - \mathbf{r}_i) + \delta(\mathbf{r} - \mathbf{r}_j)]. \tag{11}$$

In this form it is clear how the individual contributions are assigned to each particle. The kinetic contribution is at $\mathbf{r}_i$ while there are two potential contributions, one at $\mathbf{r}_i$ and the other at $\mathbf{r}_j$.

We will be interested in the total heat flux $\mathbf{J}_Q(t)$ obtained as the volume integral of Eq. (11), and the local heat current $\mathbf{J}_Q(\mathbf{r}_i,t)$ obtained from the integral over the volume assigned to particle i, that is, the integral over V_i. For the total heat flux all δ functions are contained within the integration region so

$$\mathbf{J}_Q(t)V = \sum_{i=1}^{N} U_i\mathbf{v}_i - \frac{1}{2}\sum_{i,j}^{N} \hat{\mathbf{r}}_{ij}(\hat{\mathbf{r}}_{ij}\cdot\mathbf{v}_{ij})\hat{\mathbf{r}}_{ij} \cdot(\mathbf{v}_i + \mathbf{v}_j)\delta(t - t_{ij}). \tag{12}$$

For the QOD system the local heat flux has potential contributions from two sources, either from a collision of particles i and $i+1$ or from a collision of particles $i-1$ and i. The result is

$$\mathbf{J}_Q(\mathbf{r}_i,t)V_i = U_i\mathbf{v}_i - \frac{1}{4}\sum_{j\in\{i-1,i+1\}}^{N} \hat{\mathbf{r}}_{ij}(\hat{\mathbf{r}}_{ij}\cdot\mathbf{v}_{ij})\hat{\mathbf{r}}_{ij} \cdot(\mathbf{v}_i + \mathbf{v}_j)\delta(t - t_{ij}). \tag{13}$$

Clearly the time averages of these two heat currents are the physically important quantities as the heat current must satisfy a continuity equation. But the continuity equation states that for the QOD system, on average, the same amount of heat passes through any vertical line regardless of its position. Returning to the heat current density in Eq. (9), we can define the heat current at some arbitrary x value. Instantaneously, there is only a kinetic contribution if a particle has its coordinate $x_i = x$, and there is only a potential contribution if two particles collide where for one $x_i < x$ and for the other $x_j > x$, so that the line of δ functions in Eq. (10) has 1 at position x. The time average of this instantaneous quantity must satisfy the continuity equation.

It is easy to see that summing the RHS of Eq. (13) over all particles i gives the RHS of Eq. (12), and therefore

$$\mathbf{J}_Q(\mathbf{r},t)V = \sum_{i=1}^{N} \mathbf{J}_Q(\mathbf{r}_i,t)V_i, \tag{14}$$

so that the total heat flux $\mathbf{J}_Q(\mathbf{r},t)$ is the weighted sum of local contributions with weights V_i/V. Taking the time average of both sides of Eq. (14) to obtain $\langle J_Q(\mathbf{r})\rangle_t$ and $\langle J_Q(\mathbf{r}_i)\rangle_t$, which must by the continuity equation be equal, Eq. (14) reduces to a trivial equality.

III. THE GENERALIZED GIBBS RELATION: KINETIC THEORY

The kinetic theory basis for nonequilibrium thermodynamics of the heat transport model in QOD systems has been discussed recently [19]. The basic ingredient is the kinetic contribution to the Boltzmann entropy $S(t)$ which is defined, up to a constant, to be

$$\begin{aligned} S(t) &= \int d\mathbf{r} s(\mathbf{r},t) \\ &= -\int d\mathbf{r} \int d\mathbf{v} f(\mathbf{r},\mathbf{v},t) \ln f(\mathbf{r},\mathbf{v},t), \end{aligned} \tag{15}$$

where $s(\mathbf{r},t)$ is the entropy density at position $\mathbf{r}$ at time t. We have set Boltzmann's constant to unity ($k_B = 1$). In kinetic theory the time evolution of the distribution function $f(\mathbf{r},\mathbf{v},t)$ can be obtained from the Boltzmann equation which, without external forces, takes the following form:

$$\frac{\partial f}{\partial t} + \mathbf{v}\cdot\frac{\partial f}{\partial \mathbf{r}} = J[f], \tag{16}$$

where $J[f]$ is the collision integral. The distribution function is normalized as

$$\int d\mathbf{v} f(\mathbf{r},\mathbf{v},t) = n(\mathbf{r},t), \tag{17}$$

where $n(\mathbf{r},t)$ is the local number density of the system.

The local entropy-balance equation can then be derived theoretically by substituting the time derivative of f from the Boltzmann equation (16) into the derivative of the Boltzmann entropy, Eq. (15). The result is expressed as

$$\frac{\partial s}{\partial t} + \nabla\cdot\mathbf{j}_s = \sigma, \tag{18}$$

where σ is the entropy production. In the above the entropy flux $\mathbf{j}_s$ is given exactly by

$$\mathbf{j}_s(\mathbf{r},t) = -\int d\mathbf{v}\mathbf{v} f \ln f, \tag{19}$$

but the Bhatnagar-Gross-Krook (BGK) approximation for the collision integral [23] is needed to obtain a computable form for the entropy production per unit volume σ, given by

$$\begin{aligned} \sigma(\mathbf{r},t) &= -\int d\mathbf{v} J[f] \ln f \\ &= \nu(\mathbf{r}) k \int d\mathbf{v}\{f(\mathbf{v}) - f_{loc}(\mathbf{v})\} \ln f(\mathbf{v}). \end{aligned} \tag{20}$$

The term $\nu(\mathbf{r})$ is essentially a parameter that is related to the local collision frequency given by $\nu_0 n(\mathbf{r})\sqrt{T(\mathbf{r})}$ (where ν_0 is a constant that depends on dimensionality). According to the H theorem [24] the local entropy production $\sigma(\mathbf{r},t)$ must be non-negative everywhere in the system. All the local quantities associated with the entropy-balance equation (18) have been defined through the Boltzmann equation and their definitions are exact within the validity of the Boltzmann equation and are not restricted to the linear regime.

We consider a steady system with a temperature gradient along the x direction where the average total momentum is zero, to provide a concrete theoretical description of the well-adapted linear irreversible thermodynamics for our system. In the Chapman-Enskog expansion solution to first order in the gradient (that is, Navier-Stokes order [25]) the distribution function is given by $f = f_{loc}(1+\Phi)$ where f_{loc} is the normalized local equilibrium distribution function.

The deviation from local equilibrium is obtained at the first Sonine approximation explicitly as [26,27]

$$\Phi(x,\mathbf{v}) = -\frac{m}{2}\frac{\kappa}{p}\left(\frac{mv^2}{2kT} - 2\right) v_x \frac{d\ln T}{dx}, \tag{21}$$

in which p is the hydrostatic pressure and κ is the thermal conductivity. Note that the spatial dependence of the solution occurs only through the hydrodynamic fields, in particular T, which is a well-known characteristic of a *normal* solution to the Boltzmann equation [28], and it follows that any velocity moments will possess similar dependence. Since the local energy balance in the steady state implies that $\nabla\cdot\mathbf{j}_Q(x) = 0$, the heat flux must be uniform, in contrast to the entropy balance, in which the entropy flux is nonuniform but satisfies $\nabla\cdot\mathbf{j}_s = \sigma$.

The entropy flux is given to Navier-Stokes order [29] as

$$\mathbf{j}_s(x) \simeq -k_B \int d\mathbf{v}\mathbf{v}\Phi \ln f_{loc} = -\kappa T^{-1}\frac{dT}{dx}\hat{x}. \tag{22}$$

Assuming Fourier's law, one can cast the expression for the entropy flux into the form $\mathbf{j}_s(x) = \mathbf{j}_Q(x)/T$, and the entropy production in the the steady state can be calculated from

$$\sigma(x) = \nabla\cdot\left(\frac{\mathbf{j}_Q}{T}\right) \simeq \kappa\left|\frac{d\ln T}{dx}\right|^2, \tag{23}$$

which is clearly positive. The relation between the entropy flux and the heat flux may also be viewed as a generalized version of the equilibrium Clausius relation $đQ = TdS$ extended to steady states. Whether this remains an equality, or becomes

an inequality, is central to extending thermodynamics to nonequilibrium steady states.

IV. EQUILIBRIUM

A. Dissipation and entropy production

In a previous study [12] it was shown that an energy balance is achieved for a QOD system with reservoirs of equal temperature, but that entropy is produced near each reservoir which then flows from the system to the reservoir. The observation that a system designed to be "in equilibrium" is actually dissipative is somewhat surprising, but in a sense this effect is restricted to a small region near each boundary and the bulk of the system can be regarded as in equilibrium. The entropy production is calculated from the numerically generated momentum distributions in the BGK approximation [23] and is strictly a kinetic contribution, ignoring possible configurational contributions. In Sec. II B, a dissipation is calculated from the tangent space dynamics of the system which is not limited to the kinetic regime but is rather the decrease in phase volume which leads to a negative sum of Lyapunov exponents. This dissipation is again a boundary effect as it arises from the tangent space dynamics of the collision between the reservoir and its neighboring particle. All other collision events in the dynamics give no contribution to the dissipation.

The two-dimensional momentum distributions for each particle are calculated numerically on a grid $M \times M$ with $M = 301$ typically, and a resolution of 0.05. The entropy, entropy flux, and entropy production are all calculated numerically by integrating this distribution using Eqs. (15), (19), and (26) with an error of the order of the square of the resolution, that is, 0.0025. The entropy flux and production are defined through the momentum distributions for particles and are expected to be good representations at low density in the *kinetic regime* where $\rho < 0.1$, but would neglect other potential contributions at higher density. The expression for the kinetic entropy flux is formally exact whereas the kinetic entropy production is determined in the BGK approximation.

Both the dissipation and entropy production in the system with equal reservoirs are intensive, and so largely independent of the system size, and involving only properties of the particles that are in contact with the reservoirs. The dissipation involves the collisions between the closest particle and the wall while the entropy production depends on the distribution of velocities for particles near the wall. The numerical convergence of these two quantities is quite different: the dissipation converges quite quickly with random fluctuations; the entropy production converges with the smoothness of the distributions increasing slowly and monotonically at disks 1 and N until a steady value is reached. Statistically, the distribution function needs to be sampled sufficiently to obtain a reliable value over the whole two-dimensional space (v_x, v_y) and the convergence of the local equilibrium distribution also depends on the convergence to the local properties $n(x)$, $T_x(x)$, and $T_y(x)$. For $N = 40$ and $\rho = 0.03$ the majority of the entropy production (60%) comes from particles 1 and N with 40% from the other particles (principally 2 and $N - 1$). At higher density, $\rho = 0.8$, the relationship is very similar.

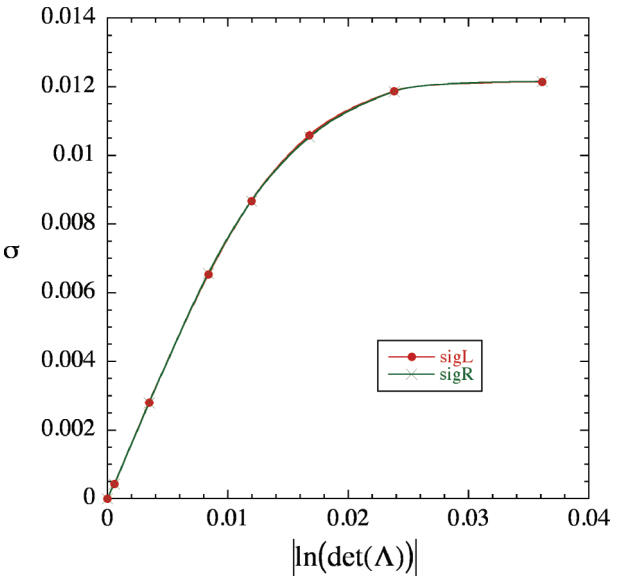

FIG. 2. (Color online) The entropy production of particles 1 and N plotted as a function of the dissipation at the left-hand reservoir (red dots) and right-hand reservoir (green crosses) for an equilibrium QOD system of 40 hard disks with $T_L = T_R = 2$ and $\rho = 0.03$. The curve is parametrized by the reservoir coupling parameter ϵ with values of $\epsilon = 0,0.1,0.3,0.5,0.6,0.7,0.8,0.9$. At $\epsilon = 0$ the system is isolated from the reservoir and both the dissipation and entropy production are zero. As the system is symmetric the same result follows for the right-hand reservoir. All results are obtained from averages over 1×10^8 collisions per particle and the results for σ are lower bounds on the correct result.

As this system with equal reservoir temperatures shows both dissipation and entropy production and both properties appear to be intensive, we look at both as functions of ϵ, the strength of the coupling of the system to the reservoir. From Fig. 2, although these properties are of opposite signs, they appear to be proportional when parametrized by ϵ.

V. NONEQUILIBRIUM SYSTEMS

We begin the study of nonequilibrium QOD systems by considering a system of 320 hard disks at two different densities: a low-density state of $\rho = 0.03$ and a high-density state of $\rho = 0.8$. The temperature of the cold reservoir on the right-hand side is kept constant at $T_R = 2$, and different values of the temperature of the left-hand reservoir T_L are used. The temperature gradient changes with the value of T_L and the number of disks, so we consider both systems with constant temperature gradient and systems with constant N. Our purpose here is to identify approximate (or possibly exact) scaling relations for the properties of the system as functions of system size N and temperature gradient ∇T, with a view to separating bulk properties from surface properties (or boundary effects).

A. Temperature profiles

We consider a nonequilibrium QOD system with $T_L = 130$ and $T_R = 2$ in both the low- and high-density states. Changing density, with fixed values of T_L and T_R, changes

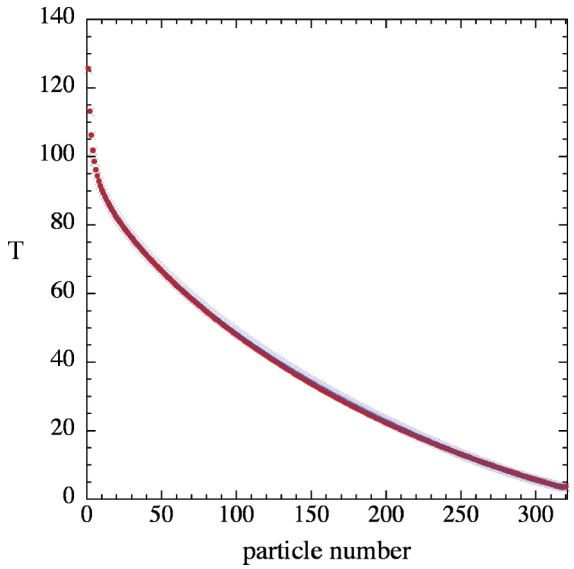

FIG. 3. (Color online) The temperature profiles (T_x) for nonequilibrium QOD systems of 320 hard disks at densities of $\rho = 0.03$ and $\rho = 0.8$. In both cases the boundary temperatures are $T_L = 130$ and $T_R = 2$. The red dots are the low-density state $\rho = 0.03$ and the blue crosses are the high-density state $\rho = 0.8$. Plotted as functions of particle number, the profiles appear almost indistinguishable, and thus imply that the profile is largely independent of density.

the temperature gradient. The two temperature profiles for T_x shown in Fig. 3 are surprisingly similar when plotted as functions of particle number, but we see in Fig. 4 that there are systematic small differences between these two profiles.

Despite the small differences seen in Fig. 3, these two profiles look quite different when plotted as functions of the average particle position x. For $\rho = 0.8$ the density does not

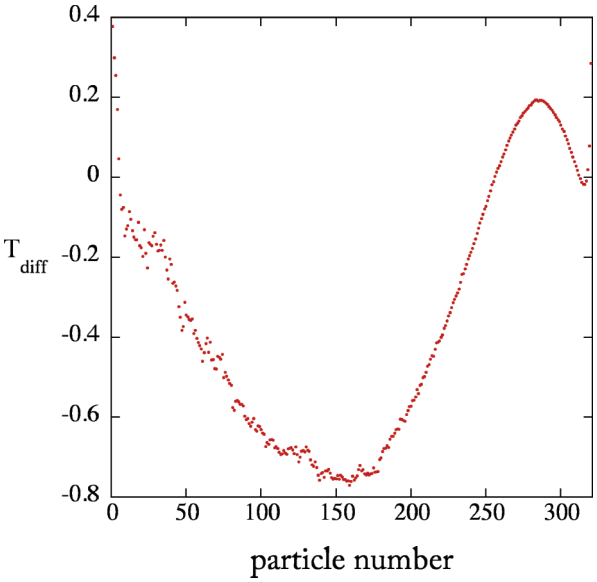

FIG. 4. (Color online) The temperature difference profiles $T_{diff} = T_x(0.03) - T_x(0.8)$ for a nonequilibrium QOD systems of 320 hard disks with $T_L = 130$ and $T_R = 2$. Despite the seeming accuracy of Fig. 3 there are small systematic differences between the two temperature profiles.

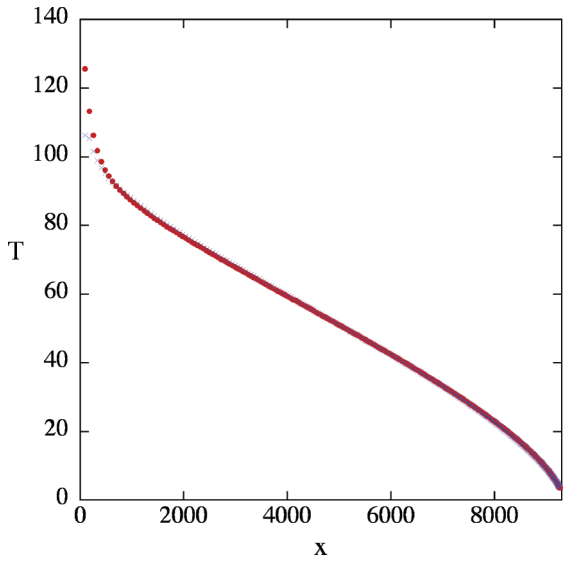

FIG. 5. (Color online) The temperature profiles T_x (red symbols) and T_y (blue symbols) for $\rho = 0.03$ for a nonequilibrium QOD system of 320 hard disks with $T_L = 130$ and $T_R = 2$ plotted as a function of average particle position $\langle x \rangle$. This profile looks quite different from that of the same system plotted as a function of particle number in Fig. 3 and appears to be approximately a cubic polynomial in x.

change greatly through the system so the profile as a function of particle number is very similar to the profile as a function of average particle position. However, for $\rho = 0.03$ the profile changes significantly, becoming closer to a polynomial in x. Notice that in Fig. 5 there is no place in the system where we could consider that the temperature profile is linear. We find that $T^{3/2}$ is close to a linear function of x, except in a region close to the left-hand reservoir. This behavior in the bulk domain is consistent with the exact results derived from the BGK model for hard spheres.

Eckmann and Young [5] derive an equation that the temperature profile should satisfy given by

$$T''(x)T(x) = \gamma[T'(x)]^2. \tag{24}$$

The parameter $\gamma = \alpha - 1$ is equal to zero for a linear temperature profile. Here for all cases considered $T''(x)$ is so small that we cannot determine a nonzero value of γ despite the obvious nonlinearity of the temperature profiles.

Recently the temperature profile near the reservoirs has been modeled as a discretized Levy random walk [30,31] and this predicts a power law meniscus effect at the boundaries. Here for a system of 320 disks at low density ($\rho = 0.03$) the temperature profile has a power law behavior at the hot reservoir where $T_x(x) = T_{x,L}x^{\mu}$ with $T_{x,L}$ a constant and the meniscus exponent $\mu \sim -0.15$. The constant $T_{x,L}$ changes with temperature gradient but the exponent μ is essentially constant. As the temperate profile as a function of particle number is independent of density (see Fig. 3), the meniscus exponent should also be independent of density.

The temperature difference profile $T_x(x) - T_y(x)$ to a good approximation satisfies a strong scaling relation that is independent of density and system size. To illustrate this we use systems of 80, 160, and 320 disks at the same temperature gradient and a different position scaling on the horizontal

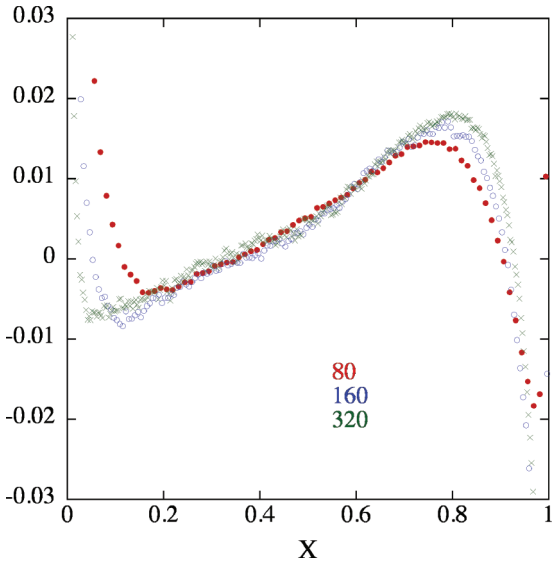

FIG. 6. (Color online) The temperature difference profile $[T_x(x) - T_y(x)]/T_x(x)$ as a function of scaled position $X = (i - \frac{1}{2})/N$ for nonequilibrium QOD systems of 80 (red filled circles), 160 (blue open circles), and 320 (green crosses) hard disks with the same temperature gradient $\nabla T = -0.013\,80$ at $\rho = 0.03$. The same graph for a density of $\rho = 0.8$ is almost identical, including its vertical scale.

axis. We take the scaled particle position $X = (i - \frac{1}{2})/N$ where i is the particle number on the horizontal axis, and plot $[T_x(x) - T_y(x)]/T_x(x)$ on the vertical axis. In Fig. 6 we notice that in the central part of the graph all curves coincide but at each end the curves change depending upon the system size. The figure for the high-density case $\rho = 0.8$ is almost identical, including the vertical scale.

B. Energy balance

The heat flux vector satisfies a continuity equation so must be, on average, constant everywhere in the system. It is composed of two parts: a kinetic part which dominates at low density, and a potential part which dominates at high density, Eq. (13). Regardless of the density, the total heat flux vector must match the energy that enters or leaves through the boundary (per unit length) by the collision mechanism Eq. (1) as this is the only way energy can enter or leave the system. As before we can calculate the energy flux through the boundary in two different ways; first a direct calculation using the collision rule at the boundary $\Delta e_L/L_y$ or $\Delta e_R/L_y$ averaged over time, and second by calculating the average heat flux J_Q which has both kinetic and potential components. In Table II we present the components of the heat flux vector and show that the energy flow through the boundaries is consistent with the heat flux calculated using Eq. (13).

C. Local energy flux

In Fig. 7 we present the components of the heat flux vector for a QOD system of 320 disks at low density where $T_L = 130$ and $T_L = 2$. Despite the large temperature gradient in this low-density state the major contribution to the heat flux comes from the kinetic term, but near the cold reservoir

TABLE II. The components of the heat flux vector J_{Qx} for QOD systems of $N = 320$ disks at two different densities and different left-hand temperatures T_L with $T_R = 2$. The superscripts K and Φ signify the kinetic and potential components, respectively. For the low-density state $\rho = 0.03$ the heat flux vector is almost completely kinetic with a very small potential contribution. In the high-density state $\rho = 0.8$ almost all of the heat flux vector is potential. Despite these differences the match between the total heat flux vector and the energy flow through the boundary is excellent.

ρ	T_L	J^K_{Qx}	J^Φ_{Qx}	J^T_{Qx}	$\Delta e_L/L_y$
0.03	6	0.002917	0.000098	0.003015	0.003015
0.03	10	0.006991	0.000234	0.00723	0.007226
0.03	34	0.04604	0.001541	0.047581	0.047584
0.03	66	0.12404	0.004151	0.1282	0.1282
0.03	130	0.3398	0.01137	0.35117	0.35124
0.8	6	0.07574	0.407122	0.48286	0.48426
0.8	10	0.1828	0.9719	1.1547	1.158
0.8	34	1.2181	6.2552	7.4733	7.4951
0.8	66	3.2850	16.547	19.832	19.889
0.8	130	8.9787	44.469	53.4477	53.6009

where the local density is greatest there is a contribution from the potential term that gives 25% of the total. The total heat flux vector is close to constant throughout the system, except for a small peak near the hot reservoir and another small increase near the cold reservoir. Apart from these boundary effects, the continuity of the local heat flux vector is very good and changes in the kinetic contribution are compensated for by changes in the potential contribution. The local kinetic contribution is equal to the local temperature

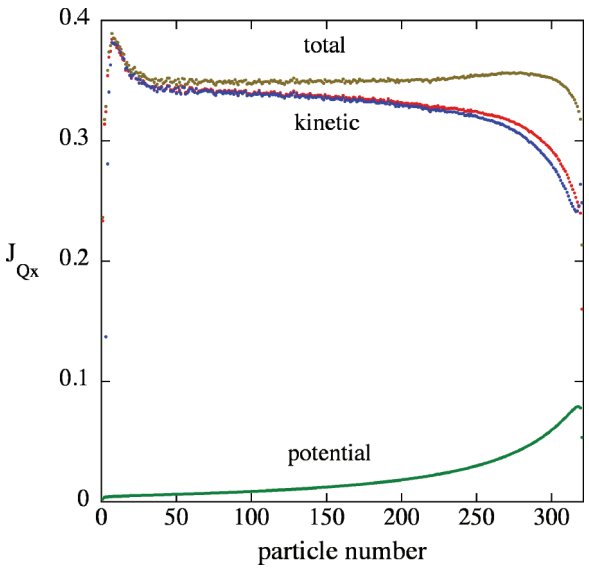

FIG. 7. (Color online) The components of the local heat flux vector for a QOD system of 320 disks at a density of $\rho = 0.03$ with $T_L = 130$ and $T_R = 2$. The red symbols are the kinetic contribution to the heat flux vector, the green symbols are the potential contribution, and the brown symbols are the total heat flux vector which must be constant throughout the system. The blue symbols are the local entropy flux times the local temperature, which is equal to the kinetic contribution to the heat flux vector almost everywhere.

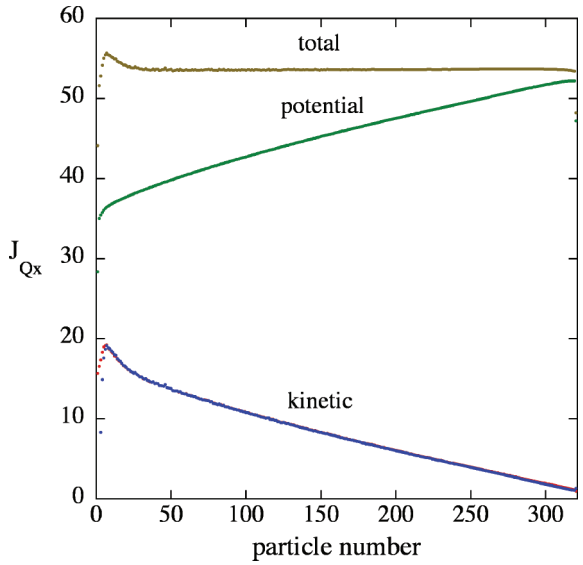

FIG. 8. (Color online) The components of the local heat flux vector for a QOD system of 320 disks at a density of $\rho = 0.8$ with $T_L = 130$ and $T_R = 2$. The red symbols are the kinetic contribution to the heat flux vector, the green symbols are the potential contribution, and the brown symbols are the total heat flux vector which must be constant throughout the system. The blue symbols are the local entropy flux times the local temperature, which is indistinguishable from the kinetic contribution to the heat flux vector everywhere.

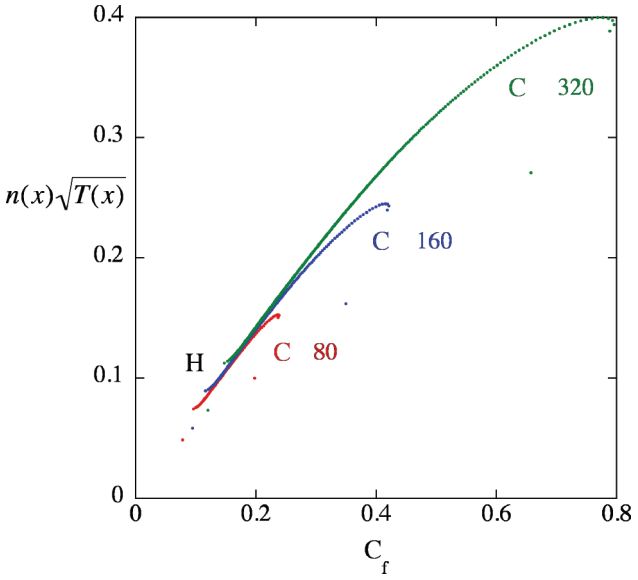

FIG. 9. (Color online) The theoretical BGK collision frequency $n(x)\sqrt{T(x)}$ plotted as a function of the directly calculated local collision frequency for systems of 80, 160, and 320 disks at a density of 0.03 and temperature gradient of $\nabla T = -0.0138$. In each case the externally applied temperature gradient is the same. The labels *H* and *C* signify the positions of the hot and cold reservoirs respectively.

times the local entropy flux except in the region near the cold reservoir. If the local velocity distribution is exactly Gaussian at the local density and temperature then $J_Q(x) = T(x)j_s(x)$. Here these two properties show systematic changes near the cold reservoir where the numerical velocity distribution must deviate sufficiently from the local equilibrium distribution.

For the higher-density state the situation is somewhat different; see Fig. 8. Here the potential contribution to the local heat flux vector dominates the kinetic contribution and near the cold reservoir there is almost no kinetic contribution. Again the local total heat flux vector is constant throughout, apart from a small peak near the hot reservoir, and the local kinetic contributions to $J_Q(x)$ and $T(x)j_s(x)$ are indistinguishable everywhere. Indeed, the agreement between the kinetic contributions is much better at high density than it is at low density in the kinetic region.

D. Local collision frequency and entropy density

In the kinetic regime we need the BGK approximation to obtain an estimate of the local entropy production and central to this is the local collisional relaxation frequency $\nu(x)$. We can test the proposition [32] that the BGK local collision relaxation frequency for hard disks is given by $\nu(x) = \nu_0 n(x)\sqrt{T(x)}$ in the kinetic regime by plotting it against the local collision frequency calculated directly. In Fig. 9, we present $n(x)\sqrt{T(x)}$ as a function of the numerical collision frequency C_f at a density of 0.03 for three different system sizes ($N = 80, 160, 320$) each with the same temperature gradient. From Fig. 9 the resulting curve is the same and approximately linear, with deviations from linear greatest near the cold reservoir where the density is highest and potential contributions are larger. Similarly, if we keep the system size fixed at $N = 320$ and consider different values of T_L, and thus different ∇T, the resulting curve is the same, and is the same as that shown in Fig. 9. The results are consistent with a single functional form $n(x)\sqrt{T(x)} = \frac{2}{3}C_f$. If we equate the BGK relaxation frequency $\nu(x)$ with the numerical collision frequency C_f then we have $\nu(x) = \frac{3}{2}n(x)\sqrt{T(x)} = C_f$. While we might expect that $n(x)\sqrt{T(x)}$ is proportional to C_f, a universal linear relation is surprising. At high densities this proportionality breaks down completely and these properties are not related in the same way.

In Sec. III, the local entropy-balance equation was derived theoretically as Eq. (18), which equates the local change in entropy density to the divergence of the entropy flux and the entropy production σ. In a steady state the local entropy density does not change so $\nabla \cdot \mathbf{j}_s = \sigma$. The kinetic entropy flux is known exactly through Eq. (25) but the entropy production involves an unknown local relaxation frequency $\nu(x)$ that is the essential ingredient in the BGK approximation for the collision integral. Using the numerical results for the entropy flux and the entropy production [assuming that $\nu(x) = \nu_0 n(x)\sqrt{T(x)}$] we can estimate ν_0 as the slope of a best-fit line. The entropy-balance equation can be written as

$$\frac{\partial}{\partial x} j_{Sx}(x) = \nu_0 n(x)\sqrt{T(x)} \int d\mathbf{v}\{f(\mathbf{v}) - f_{loc}(\mathbf{v})\} \ln f(\mathbf{v}), \tag{25}$$

where the left-hand side can be calculated, and all of the right-hand side, except for ν_0, can be calculated, so the self-consistent ν_0 value is the slope of the line. We exclude the region nearest tho two reservoirs (approximately ten particles on each side), and the resulting curve is approximately linear with the slopes given in Table III for different values of

TABLE III. The self-consistent estimate of the value of ν_0 from the local entropy flux and BGK entropy production using QOD systems of 320 disks at a density $\rho = 0.03$ with the right-hand reservoir temperature of $T_R = 2$ for a range of values of the left-hand reservoir temperature T_L.

T_L	ν_0
18	0.295
34	0.232
66	0.229
130	0.218

the left-hand reservoir temperature T_L. This is a direct test of the accuracy of the BGK approximation, or a self-consistent calculation of ν_0. The results are similar for all temperatures but different from the value obtained by relating $\nu(x)$ to the numerical collision frequency.

Where there is the possibility of a difference between the local values of T_x and T_y, we can use an appropriately modified local equilibrium distribution function of the form

$$f_{loc}^{M}(x,\mathbf{v}) = \frac{mn}{2\pi}\left(\frac{1}{T_x T_y}\right)^{1/2} \exp\left[-\frac{m}{2}\left(\frac{v_x^2}{T_x}+\frac{v_y^2}{T_y}\right)\right]. \quad (26)$$

Here n, T_x, and T_y are the local number density and x and y components of the temperature, which are all functions of position x. The entropy density obtained from this modified local equilibrium distribution is

$$s_{loc}^{M}(x) = n\left[1 - \ln\left(\frac{mn}{2\pi}\right) + \frac{1}{2}\ln(T_x T_y)\right], \quad (27)$$

which is reminiscent of the equilibrium Sackur-Tetrode equation except that here the hydrodynamic fields are local. While the exact momentum distributions for the particles cannot be exactly Gaussian as this nonequilibrium system supports an energy current, the deviations from Gaussian are at best only subtle and the local entropy density calculated from the numerical momentum distributions is almost indistinguishable from the local entropy density calculated from the modified local equilibrium distribution. The results in Fig. 10 illustrate this for systems of 320 disks for a range of different temperature gradients.

E. Local-entropy production and flux

The entropy production for a nonequilibrium steady state will be generated throughout the system wherever the particle momentum distribution differs from the local equilibrium distribution. The continuity of the heat flux vector throughout the system ensures that there are deviations from the local equilibrium momentum distribution at the position of each particle, giving rise to local entropy production everywhere. This ubiquitous entropy production leads to an associated entropy flux towards the reservoirs, in addition to that observed at equilibrium, which will bias and add nonequilibrium effects to the equilibrium baseline. While the momentum distributions for the particles are perturbed from Gaussian because of the energy current, the deviations from Gaussian are small and at best subtle. The numerical convergences of the integrations

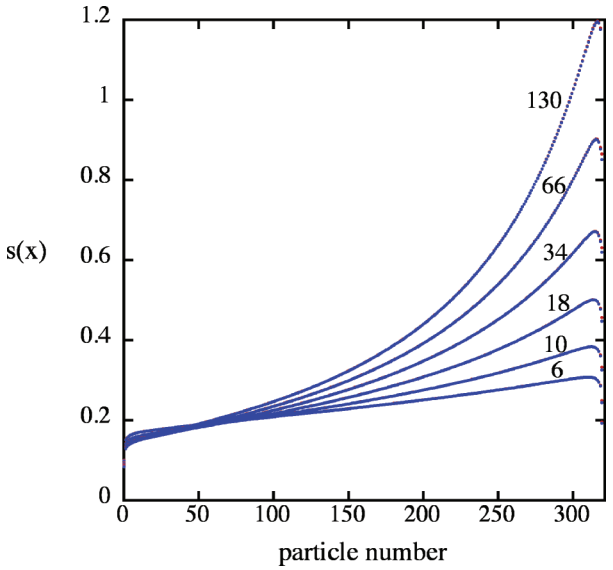

FIG. 10. (Color online) The local entropy density $s(x)$ calculated from the numerical momentum distributions (blue symbols) and from the local equilibrium distribution (red symbols) plotted as functions of the particle number for systems of 320 disks at a density of 0.03. The label on each curve is T_L. For each temperature gradient the agreement is excellent.

required for these two properties are quite different. The local entropy flux converges very quickly while the local entropy production, which is necessarily positive, is quite slow to converge and can have negative regions which take a very long time to decay to zero. Indeed, the dominant boundary entropy production terms for particles 1 and N seem to increase uniformly as they converge. In other regions, away from the reservoirs, the local entropy production decreases as it converges.

For a QOD system of 320 disks at density $\rho = 0.03$, shown in Fig. 11, we see systematic changes in the local entropy production σ_{ent}/ν as the value of T_L changes. For T_L up to values of about 10 the changes are restricted to a lift in the baseline with a small positive slope. For larger values of T_L the changes are less systematic and at large values 66 and 130 a negative region appears near the hot reservoir. For the same system the local entropy flux shown in Fig. 12 has systematic changes for all values of T_L up to the largest considered, of 130. As before, the baseline is positive (away from the reservoirs) and increases with increasing particle number and with increasing T_L. Clearly the fact that j_S is positive implies that the current of entropy is always directed to the right-hand cold reservoir in the center and on the right-hand side but the value of the entropy flux for particle 1 does not change with T_L despite the fact that this is the boundary where the temperature changes. Similarly, the entropy production at this wall is relatively constant with larger changes on the right-hand side.

All calculations of entropy, entropy flux, or entropy production consider only the kinetic contributions. These considerations are likely to be accurate for low-density systems where we can assume that the potential contributions are small so we consider the low-density QOD system with $T_R = 2$ and a range of left-hand reservoir temperatures T_L. As the boundaries themselves, and the boundary layer, create entropy

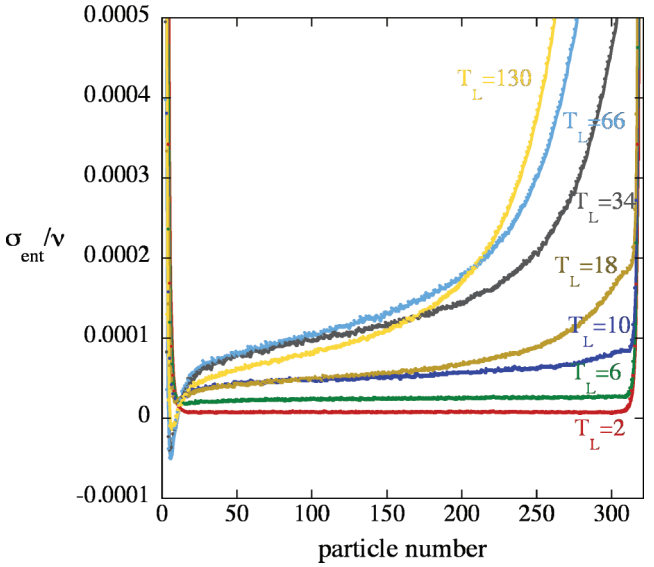

FIG. 11. (Color online) The local kinetic entropy production divided by ν plotted as a function of particle number for QOD systems of 320 disks at a density of 0.03 with the right-hand reservoir at temperature $T_R = 2$ for various values of temperature gradient (or left-hand reservoir temperature T_L).

production and flux we ignore boundary effects by considering the bulk system to begin at $N = 10$ and end at $N = 310$, for the 320-particle system. We know that the heat flux vector is consistent with the heat flow across the boundaries so we work from the heat flux to calculate entropy fluxes and compare those with the ones calculated directly.

The first row of Table IV contains the numerical values of the local temperature and kinetic entropy flux j_S calculated directly in the simulation. The local Clausius equality $j_S = J_Q/T$ suggests that the entropy flux can also be calculated from the ratio of the heat flux vector J_Q and the local temperature, which are both accurately known in the simulation. If the

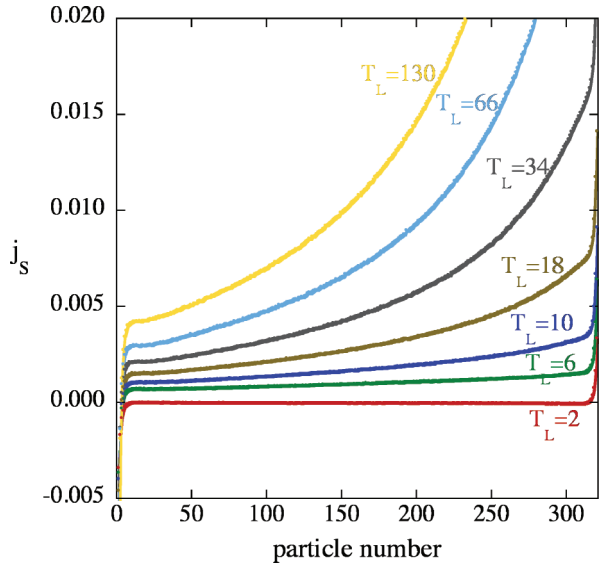

FIG. 12. (Color online) The local kinetic entropy flux for the same systems as in Fig. 11.

TABLE IV. The local temperature, entropy, and energy flux for a QOD system of 320 disks at low density 0.03 with reservoir temperatures $T_R = 2$ and a range of values of T_L. We combine the reservoir and the nearest 9–10 disks and consider the system explicitly at particle 10 and particle $N = 310$.

T_L	T_{10}	$j_{S,10}$	J_Q/T_{10}	T_{310}	$j_{S,310}$	J_Q/T_{310}
10	7.4357	0.001059	0.000971	2.0555	0.003394	0.003513
18	13.062	0.00156	0.001394	2.3201	0.007353	0.007849
34	24.215	0.00214	0.001968	2.7333	0.015299	0.017433

Clausius equality holds then we expect that $j_{S,10} = J_Q/T_{10}$ and $j_{S,310} = J_Q/T_{310}$. We can see that at particle 10 near the hot reservoir this is a slight underestimate of J_Q/T_{10} and at particle 310 the value of J_Q/T_{310} is an overestimate, possibly due to potential contributions, as the density is higher near the cold reservoir. The results in Table IV show that at low density, ignoring the boundary layer, the heat flux vector and the kinetic entropy flux agree reasonably well. For higher densities, such as $\rho = 0.8$, the potential contributions to the entropy flux that are implied by the values of J_Q/T suggest that the kinetic entropy flux is only a small part of the total entropy flux and we would not expect agreement.

F. Phase space contraction and entropy production

The system is in a nonequilibrium steady state with a local entropy production that we can estimate using the BGK approximation. The phase space contraction, as before for the equal-reservoir case, can be calculated from the tangent space dynamics and will contribute only at the collisions of particles with the boundaries. Here the different reservoir temperatures break the reflection symmetry and hence both the left- and right-hand-side phase space contractions will be different, as will the entropy productions for particles 1 and N. We might imagine that the local entropy production and phase space contraction at each boundary may match separately but this is not what we observe. The phase space contraction calculated from the tangent space dynamics of the particle nearest each reservoir converges quite rapidly, and although the dissipation will be an extensive quantity, the whole process takes places at the boundaries, mostly at the cold reservoir. At the cold reservoir the local density is highest and the collision frequency is highest but the average particle velocity is smallest. At the hot reservoir the local density is lowest and the collision frequency lowest but the average particle velocity is highest.

Here we concentrate on a series of simulations at constant $N = 320$ and $\rho = 0.03$ and $\rho = 0.8$ to identify the dependence of the phase space contraction and boundary entropy productions σ_1 and σ_N on the temperature gradient. The results for both densities are presented in Fig. 13 and the results are complicated. We note that the phase-space contraction is negative whereas the entropy production is positive.

Points to note about Fig. 13 are that when the reservoir temperatures are symmetric, with, for example, $T_L = T_R = 2$, neither the phase space contraction nor the entropy production at 1 or N is zero, so this system is always dissipative. Both of these effects are caused by the boundary condition that is applied at each reservoir boundary. The phase space

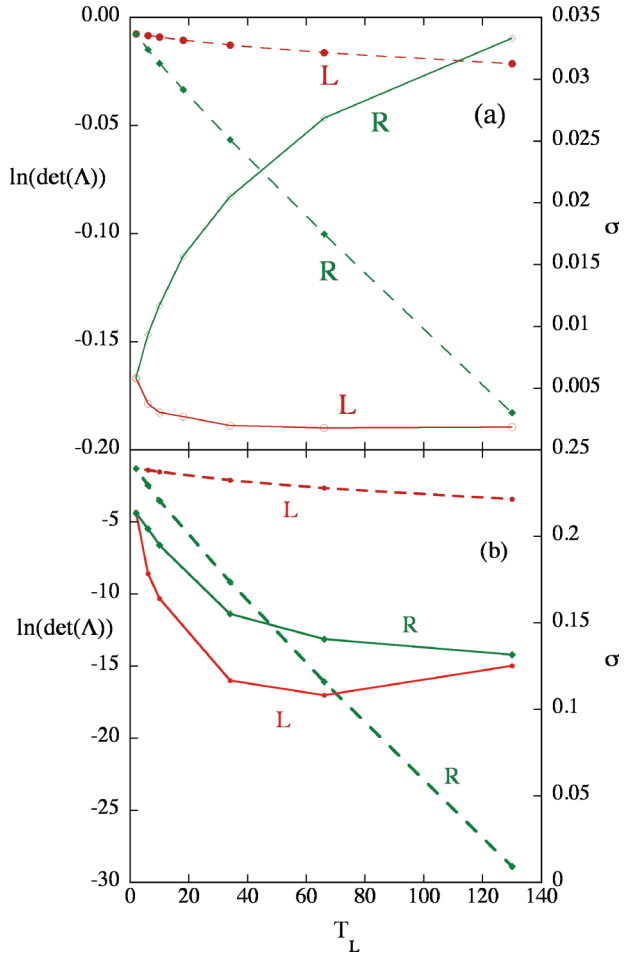

FIG. 13. (Color online) Phase space contraction ln[det(Λ)] and entropy production σ at disk 1 (labelled L) and N (labeled R) for QOD systems of 320 disks with the right-hand reservoir temperature fixed at $T_R = 2$ for a range of values of the left-hand reservoir temperature $2 \leqslant T_L \leqslant 130$. (a) is the result for a density $\rho = 0.03$ and (b) is for a density $\rho = 0.8$. The filled symbols are values of the dissipation ln[det(Λ)] and the empty symbols are values of σ. The red symbols are for the left-hand reservoir and the green symbols are for the right-hand reservoir.

contractions for both densities are essentially linear in the reservoir temperatures T_L and T_R, and the slope (or magnitude) is greatest at the cold reservoir where the collision rate is largest. The ratio of the slopes T_R/T_L is also remarkably independent of density.

The entropy productions at 1 and N are initially the same for $T_L = 2$ but thereafter change systematically with T_L but differently with density. At low density σ_1 decreases while σ_N increases quickly with increasing T_L. Here it is tempting to associate ln[det(Λ_R)] and σ_N, but at the hot reservoir ln[det(Λ_L)] and σ_1 change in different directions.

At high density both σ_1 and σ_N decrease with increasing T_L. So the proportionality of ln[det(Λ_R)] and σ_N observed for equal reservoir temperatures disappears when the temperatures differ, and is even more different at high density.

The results presented in Fig. 13 are for the phase space contraction and entropy production as functions of T_L or equivalently the temperature gradient. We have also studied these properties as functions of system size N at fixed temperature gradient and here the graphs are very similar to those in Fig. 13. If we do a linear fit to the phase space contraction as a function of N and find slopes α_L and α_R, respectively (for the L and R reservoirs), and then do a linear fit to the phase space contraction as a function of T_L and find the slopes β_L and β_R, then we find the relations in Table V.

TABLE V. The relationship between the slopes of linear fits to the phase space contraction as functions of N and T_L.

ρ	α_R/α_L	β_R/β_L	α_L/β_L	α_R/β_R
0.03	9.1	12.7	56	79
0.8	10.4	12.95	66.5	82.7

The graphs of the entropy production σ as functions of N and T_L are also very similar but as they are not linear we cannot repeat the analysis above. However, we can deduce from Table V that at $\rho = 0.8$ the functional form of ln[det(Λ_L)] as a function of T_L can be obtained from the functional form as a function of N by replacing N by $66.5T_L$. Similarly, the functional form of $\sigma_L(N)$ gives the functional form as a function of T_L by replacing N by $43T_L$. These results are qualitatively the same for the low density $\rho = 0.03$ with only small changes in numerical factors.

G. Thermal conductivity

Lower-dimensional systems have long been shown to exhibit anomalous thermal conductivity with typically a power

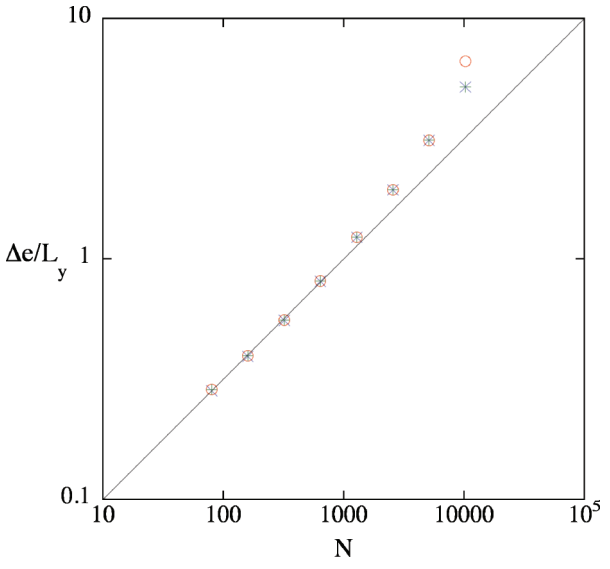

FIG. 14. (Color online) A log-log plot of the heat flux calculated in three independent ways as a function of N for QOD systems at a density of $\rho = 0.8$ and temperature gradient of $\nabla T = -0.368$ for a large range of system sizes. The right-hand reservoir temperature is fixed at $T_R = 2$ and T_L varies such that ∇T remains fixed. The red open circles are values of the heat flux into the system through the left-hand boundary $\Delta e_L/L_y$, the green pluses are the values of the heat flux out of the system through the right-hand boundary $\Delta e_R/L_y$, and the blue crosses are the values calculated from the heat flux vector J_Q (13). The line corresponds to $\Delta e = N^{1/2}$.

law divergence of the form N^{α} where $0.33 < \alpha \leqslant \frac{1}{2}$. The QOD system is a restricted two-dimensional system where the average momentum is equal to zero, so we might expect two-dimensional behavior, or perhaps marginally below two-dimensional. In Fig. 14 we have a result that suggests that $\alpha \geqslant \frac{1}{2}$ although extrapolation to large N is always problematic. The numerical convergence of this system at fixed N suggests that the initial value of the heat flux is high and then this converges slowly to a smaller value. Ideally, we may try to have the number of collisions per particle fixed for each system size but this is difficult for larger systems as the total run time increases at least as fast as N^2. Therefore the accuracy of the results decreases quickly for large system sizes. The consistency of the different routes to the heat flux gives a good indication of the convergence of the result, so the result for $N = 10\,240$ is the least reliable of those reported in Fig. 14.

VI. CONCLUSION

We have investigated the consequences of a particular model microscopic coupling of a system to a reservoir. The advantages of the model include its relative simplicity and the fact that it is deterministic, which allows straightforward application of dynamical system techniques. Clearly the fact that the particles remain ordered from left to right, and that this allows us to connect the properties of a volume element with the properties of a single particle, is a virtue of the quasi-one-dimensional system. In more realistic systems this is not possible as particles enter and leave Eulerian volume elements, but the generalization is a technical rather than a conceptual difficulty.

The microscopic expression for the local heat flux vector derived here has been shown to satisfy the expected continuity equation for heat flow at both low density, where kinetic contributions dominate, and high density, where potential contributions dominate. The heat flux vector also agrees very well with the amount of energy entering the system from the left-hand reservoir and the amount of energy leaving via the right-hand reservoir.

Strong scaling relations were obtained for the temperature profile as a function of particle number and for local temperature differences. These results suggest that the system behaves more simply than expected with regard to changes in density and temperature gradient.

The entropy terms calculated here are all kinetic contributions and would not be expected to match at high densities although the kinetic contributions to the heat flux vector match the temperature times the kinetic contribution to the entropy flux. As potential contributions to the heat flux vector are large at high densities we would expect large potential contributions to the various entropy terms, including its production and flux, to be present.

[1] T. Prosen and D. K. Campbell, Phys. Rev. Lett. **84**, 2857 (2000).
[2] P. Grassberger, W. Nadler, and L. Yang, Phys. Rev. Lett. **89**, 180601 (2002).
[3] S. Lepri, R. Livi, and A. Politi, Phys. Rep. **377**, 1 (2003).
[4] D. K. Campbell, P. Rosenau, and G. M. Zaslavsky, Chaos **15**, 015101 (2005).
[5] J.-P. Eckmann and L. S. Young, Europhys. Lett. **68**, 790 (2004); Commun. Math. Phys. **262**, 237 (2006).
[6] P. Collet and J.-P. Eckmann, Commun. Math. Phys. **287**, 1015 (2009).
[7] P. Collet, J.-P. Eckmann, and C. Mejia-Monasterio, J. Stat. Phys. **136**, 331 (2009).
[8] J. M. Deutsch and O. Narayan, Phys. Rev. E **68**, 010201 (2003); **68**, 041203 (2003).
[9] A. Lipowski and D. Lipowska, Phys. Rev. E **75**, 052201 (2007); S. Woloszczuk and A. Lipowski, *ibid.* **81**, 061132 (2010).
[10] E. Ott, Chaos in Dynamical Systems (Cambridge University Press, Cambridge, 1993).
[11] T. Taniguchi and G. P. Morriss, C. R. Phys. **8**, 625 (2007).
[12] G. P. Morriss and D. Truant, Entropy **14**, 1011 (2012).
[13] D. J. Evans and G. P. Morriss, *Statistical Mechanics of Nonequilibrium Liquids*, 2nd ed. (Cambridge University Press, Cambridge, 2008).
[14] A. Baranyai, Phys. Rev. E **61**, 3306 (2000); **62**, 5989 (2000).
[15] D. J. Evans, J. Stat. Phys. **57**, 745 (1989).
[16] G. P. Morriss and L. Rondoni, Phys. Rev. E **59**, 5 (1999).
[17] F. Ritort, J. Phys. Chem. B **109**, 6787 (2005); A. Garriga and F. Ritort, Phys. Rev. E **72**, 031505 (2005).
[18] G. P. Morriss, T. Chung, and C. Angstmann, Entropy **10**, 786 (2008).
[19] C. S. Kim and G. P. Morriss, Phys. Rev. E **80**, 061137 (2009).
[20] T. Taniguchi and G. P. Morriss, Phys. Rev. E **68**, 026218 (2003).
[21] G. P. Morriss and D. P. Truant, J. Phys. A **46**, 254010 (2013).
[22] J. A. McLennan, *Introduction to Non-Equilibrium Statistical Mechanics* (Prentice-Hall, Englewood Cliffs, NJ, 1989).
[23] R. Zwanzig, *Nonequilibrium Statistical Mechanics* (Oxford University Press, New York, 2001).
[24] C. Cercignani, *The Boltzmann Equation and Its Applications* (Springer, New York, 1988).
[25] J. R. Dorfman and H. van Beijeren, in *Statistical Mechanics, Part B: Time-Dependent Processes*, edited by B. Berne (Plenum, New York, 1977).
[26] A. Santos, J. J. Brey, and V. Garzo, Phys. Rev. A **34**, 5047 (1986); A. Santos, J. J. Brey, C. S. Kim, and J. W. Dufty, *ibid.* **39**, 320 (1989).
[27] V. Garzó and A. Santos. *Kinetic Theory of Gases in Shear Flows* (Kluwer Academic, Dordrecht, 2003).
[28] C. S. Kim, J. W. Dufty, A. Santos, and J. J. Brey, Phys. Rev. A **39**, 328 (1989).
[29] D. Jou, J. Casas-Vazquez, and G. Lebon, *Extended Irreversible Thermodynamics* (Springer, Berlin, 2001).
[30] S. Lepri and A. Politi, Phys. Rev. E **83**, 030107 (2011).
[31] A. Dhar, K. Saito, and B. Derrida, Phys. Rev. **87**, 010103 (2013).
[32] C. S. Kim and J. W. Dufty, Phys. Rev. A **40**, 6723 (1989).